Nonuniform Collimator Sensitivity: Improved Precision for Quantitative SPECT

Marie Foley Kijewski, Stefan P. Müller and Stephen C. Moore

Department of Radiology, Brigham and Women's Hospital, Boston, Massachusetts; University Medical Center, Essen, Germany; Nuclear Medicine Service, Brockton/West Roxbury VA Medical Center, Boston, Massachusetts; and Harvard Medical School, Boston, Massachusetts

Attenuation of photons degrades both the accuracy and the precision of SPECT images; attenuation correction algorithms correct the bias but cannot improve precision. Increased noise due to photon attenuation is most pronounced in regions deep in solid body sections, such as the brain and abdomen. We have quantified the degradation in performance in several estimation tasks that can be attributed to photon attenuation and determined the degree to which performance might be improved by a collimator with a nonuniform sensitivity profile. **Methods:** The analysis used ideal-observer models of performance in tasks involving estimation of the activity and size of a focal lesion. The models were based on the Cramer-Rao lower bound on the variance with which lesion activity and size can be estimated by an unbiased procedure. To quantify the effects of attenuation, values of the Cramer-Rao bound were calculated for each estimation task as a function of location of the lesion in circularly-shaped attenuators of 10- and 20-cm radii, with and without attenuation. Values of the bound were also determined for two nonuniform sensitivity profiles, one of which was designed to equalize (or nearly equalize) task performance throughout the image. **Results:** For ^{99m}Tc, photon attenuation increased the variance of the estimates by factors of up to 4.5 for the 10-cm radius attenuator and up to 20.0 for the 20-cm radius attenuator. A collimator with a nonuniform sensitivity function reduced variance by factors of up to 1.8 for the 10-cm radius attenuator and up to 2.8 for the 20-cm radius attenuator. These gains in estimation performance were insensitive to the imaging task and to deviations from the assumed attenuator size and shape. **Conclusion:** Performance in estimation tasks using images from SPECT systems with uniform sensitivity collimators is considerably lower than the theoretical optimum. We have derived a sensitivity function, realizable using existing technology, that improves performance substantially.

Key Words: quantitative SPECT; photon attenuation; collimator design; ideal-observer models; estimation

J Nucl Med 1997; 38:151–156

Attenuation of photons emitted from internal structures limits the utility of SPECT images for quantitative tasks. Photon attenuation degrades the reconstructed image in two ways: the reconstructed activity values are biased and image noise is increased. Accuracy can be improved by any of several approaches to attenuation correction, and it has been established that for homogeneous attenuators with convex external boundaries several intrinsic attenuation correction methods yield unbiased images (*1–5*). Attenuation correction methods do not address the increase in noise due to loss by attenuation of emitted photons. Like all image reconstruction and processing techniques, these methods can, at best, use the measured data optimally to achieve the lowest possible image noise given the detected data.

Received May 22, 1995; revision accepted Apr. 17, 1996.

For correspondence or reprints contact: Marie Foley Kijewski, ScD, Department of Radiology, Brigham and Women's Hospital, 75 Francis St., Boston, MA 02115.

The fundamental noise characteristics of the image can be altered only by a modified data collection strategy. Such a strategy was proposed for a dedicated brain instrument with a cylindrical detector by Genna and Smith (*6*), who suggested varying the sensitivity along the collimator so that relatively more photons are detected near the center of the projection. This concept can also be realized for planar detection systems. Variable focusing collimators (*7*) are characterized by a centrally peaked sensitivity profile, although their advantages in the current context have not been previously recognized.

In this report we investigate the effects of nonuniform collimator sensitivity on estimating activity concentration and size of a focal lesion using ideal-observer models of these imaging tasks. Models of task performance have been used to analyze various aspects of medical imaging systems (*8*), using both tasks such as lesion detection that involve human perception (*9,10*) and objective quantitation tasks (*11–13*). We have previously proposed models of performance in multiparameter estimation tasks as bases for design and optimization of SPECT systems (*14–18*). Performance in these tasks can be quantified by the accuracy and precision of an optimal procedure based on maximum-likelihood (*14*) or Bayesian estimation (*17*), or by the Cramer-Rao lower bound (CRB) (*19*) on the variance of unbiased estimates of signal parameters (*15,16,18*).

Here we have taken the latter approach, determining the CRB for estimation of activity concentration and size of a small lesion embedded in an attenuating phantom. We quantify the degradation in estimation task performance due to photon attenuation as a function of position in an attenuator. We then determine the extent to which performance can be improved by an alternative data collection strategy (i.e., using a collimator with a nonuniform sensitivity profile). We derive a sensitivity profile that equalizes task performance throughout a brain-sized attenuator, and investigate the effects on estimation performance of deviations of the anatomic contour from the assumed attenuator size and shape.

Several simplifying assumptions have been made in the analysis. We have assumed that resolution is constant along the projection and unaffected by the change in collimator sensitivity; this is true for the collimator designed by Genna and Smith (*6*). The distance-dependence of the point-spread function (PSF) has been ignored. We have also assumed that all unattenuated photons are detected. Our analysis is two-dimensional; we assume that both the object and the collimator sensitivity are constant axially. In order to isolate the effects of attenuation, we have ignored the detection of scattered radiation, and we have not addressed sampling issues.

The analysis and, consequently, the results and conclusions are based on a theoretical model of performance in estimation tasks. The performance predicted by the CRB is sometimes, but not always, achievable in practice (*18*). Therefore, the improve-

ments predicted by our analysis may not be achieved by all estimation procedures under all conditions.

MATERIALS AND METHODS

Estimation Models and the Cramer-Rao Bound

We evaluated the CRB for estimation of activity concentration and size of a disk-shaped lesion as a function of radial location in a circular, homogeneous attenuator. In the analysis below, it is assumed that background activity is not present (see, however, comments on extended radiation sources in the Discussion). In order to quantify the degradation in estimation performance due to photon attenuation, values of the CRB were determined under two conditions: a theoretical situation in which all emitted photons escape the attenuator and the actual situation in which some photons are attenuated. The projections were blurred by the projection of a Gaussian PSF, assumed constant throughout the image. The unattenuated sinogram for the lesion centered at polar coordinates (s, 0) is given by:

$$p(x, \phi) = 2A\sqrt{r^2 - (x - s\cos\phi)^2}\ \text{rect}\left(\frac{x - s\cos\phi}{2r}\right) \times CS(x) * \frac{1}{\sqrt{2\pi}\sigma}\exp\left(-\frac{x^2}{2\sigma^2}\right) \quad \text{Eq. 1}$$

and the attenuated sinogram by:

$$p_a(x, \phi) = \frac{2A}{\mu}\exp\left[-\mu\left(\sqrt{r_0^2 - x^2} - s\sin\phi\right)\right] \times \sinh\left[\mu\sqrt{r^2 - (x - s\cos\phi)^2}\right] \times \text{rect}\left(\frac{x - s\cos\phi}{2r}\right) CS(x) * \frac{1}{\sqrt{2\pi}\sigma}\exp\left(-\frac{x^2}{2\sigma^2}\right), \quad \text{Eq. 2}$$

where x and ϕ are the spatial and angular coordinates of the sinogram, A is the activity concentration of the lesion, r is its radius, r_o is the radius of the circularly-shaped phantom, σ is the width of the Gaussian PSF and μ is the linear attenuation coefficient. The rect (x) (*20*) is equal to 1 for $|x| < 1/2$ and 0 otherwise. CS(x) is the collimator sensitivity function (see below) and * denotes one-dimensional convolution. For an attenuator of elliptical cross-section, with semiaxes r_a and r_b lying along the y and x axes of the coordinate system, Equation 2 becomes:

$$p_a(x, \phi) = \frac{2A}{\mu}\exp\left\{-\mu[f(r_a, r_b, x, \phi) - s\sin\phi]\right\} \times \sinh\left[\mu\sqrt{r^2 - (x - s\cos\phi)^2}\right] \times \text{rect}\left(\frac{x - s\cos\phi}{2r}\right) CS(x) * \frac{1}{\sqrt{2\pi}\sigma}\exp\left(-\frac{x^2}{2\sigma^2}\right), \quad \text{Eq. 3}$$

where

$$f(r_a, r_b, x, \phi) = \frac{(r_b^2 - r_a^2)x\sin\phi\cos\phi + r_b r_a\sqrt{r_a^2\cos^2\phi + r_b^2\sin^2\phi - x^2}}{r_a^2\cos^2\phi + r_b^2\sin^2\phi}. \quad \text{Eq. 4}$$

The estimation models assume that one or more parameters in the above equation are unknown and must be estimated from the projection data. In this report we consider two models: a model with one unknown parameter, lesion activity concentration (A), and a two-parameter model in which both lesion activity concentration and lesion radius (A and r) are considered unknown. The first model is associated with one estimation task, termed signal-known-exactly (SKE) estimation; this is a linear task, because the data are linear in the unknown parameter, A. The second model is associated with two tasks, activity estimation with unknown size and size estimation with unknown activity; these are considered nonlinear tasks because the data are nonlinear in one of the unknown parameters, r. The CRB on variance of estimates of the unknown parameters is given by the diagonal elements of the inverse of Fisher's information matrix. For additive Poisson noise of variance equal to the expected value of the sinogram, the entries of the information matrix are given by:

$$J_{ij} = \sum_x \sum_\phi \frac{\partial p(x, \phi; \vec{\theta})}{\partial\theta_i}\frac{\partial p(x, \phi; \vec{\theta})}{\partial\theta_j}\frac{1}{p(x, \phi; \vec{\theta})}, \quad \text{Eq. 5}$$

where $\vec{\theta}$ is the vector of unknown parameters; $\vec{\theta}$ = (A) for the one-parameter model and $\vec{\theta}$ = (A, r) for the two-parameter model. The summation is over the sampled sinogram; ϕ ranges from 0 to 2π, while x ranges from −10 cm to +10 cm for the smaller attenuator and from −20 cm to +20 cm for the larger attenuator.

Collimator Sensitivity Profiles

Three collimator sensitivity profiles were considered: the standard uniform profile, in which sensitivity is constant along the projection, and two sensitivity functions that are peaked at the center of the projection. The nonuniform sensitivity profiles were normalized so that integrated sensitivity along the projection was equal to that of the uniform profile. The exponential sensitivity profile is given by:

$$CS_e(x) = K_e\exp\left(\mu\sqrt{r_0^2 - x^2}\right), \quad \text{Eq. 6}$$

where r_o is the radius of the assumed circularly-shaped attenuator and K_e is the normalization constant. For a circular attenuator of radius r_o, the exponential profile accomplishes physically the mathematical operation that is the first step in all intrinsic attenuation-correction algorithms (i.e., multiplication of each measured projection by a function that compensates for photon attenuation between a line through the center of rotation, parallel to the detector, and the external (convex) object contour nearest the detector). The exponential-cosine sensitivity profile equalizes, over all source locations, the total counts in the sinogram for a point source in a centered, circularly-shaped attenuator. The exponential-cosine sensitivity profile,

$$CS_{ec}(x) = K_{ec}\exp\left(\mu\sqrt{r_0^2 - x^2}\right)\cos(\mu x), \quad \text{Eq. 7}$$

where K_{ec} is the normalization constant, is derived in the Appendix.

The three collimator sensitivity profiles are shown in Figure 1A for the 10-cm radius attenuator and the narrow-beam attenuation coefficient of ^{99m}Tc (μ = 0.15 cm^{-1}). For a 20-cm radius attenuator, the exponential-cosine sensitivity profile of equation (*7*) is unrealizable because $\cos(\mu x) < 0$ for $|\mu x| > \pi/2$. Therefore, for the large attenuator we have modified the exponential-cosine sensitivity profile by linear combination with a function in which the argument of the cosine is replaced by $\pi x/2r_0$. The modified exponential-cosine sensitivity profile,

$$CS_{mec} = K_{mec}\exp\left(\mu\sqrt{r_0^2 - x^2}\right)\left[\left(1 - \left(\frac{|x|}{r_0}\right)^{3/2}\right)\cos(\mu x) + \left(\frac{|x|}{r_0}\right)^{3/2}\cos\left(\frac{\pi x}{2r_0}\right)\right], \quad \text{Eq. 8}$$

does not perfectly equalize sensitivity within the attenuator but is both nonnegative for $x < r_0$ and more centrally peaked than the

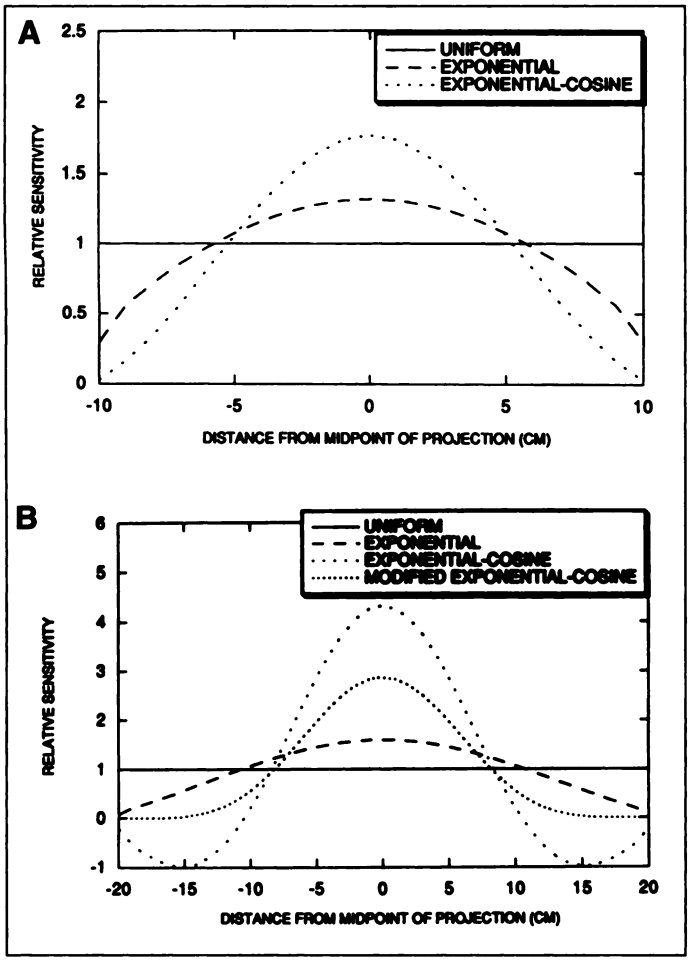

FIGURE 1. Collimator sensitivity profiles for a 10-cm (A) and 20-cm radius (B) attenuator. Profiles are normalized for equal sensitivity integrated over the projection. For the 20-cm radius attenuator, the exponential-cosine sensitivity profile is physically unrealizable.

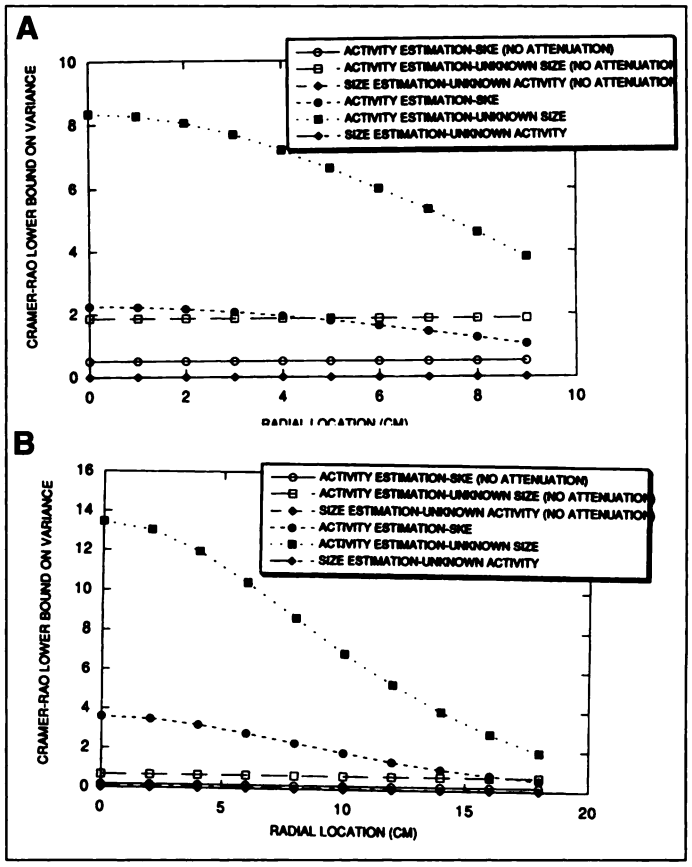

FIGURE 2. Performance in estimating activity concentration and size of a disk-shaped lesion as a function of radial location in a 10-cm (A) and 20-cm (B) radius attenuator with a uniform collimator sensitivity profile. Open symbols denote performance achievable in the absence of attenuation; closed symbols denote performance with attenuation.

exponential profile. The weighting scheme of Equation 8 is arbitrary, and other choices might more nearly equalize sensitivity. The sensitivity profiles for the 20-cm radius attenuator are shown in Figure 1B.

Calculations

Fisher's information matrix was calculated for the two estimation models, the two attenuator sizes and three sensitivity profiles for locations ranging from the phantom center to its periphery, both for an attenuation coefficient of 0.15 cm^{-1} and for no attenuation. For the 10-cm radius attenuator, the activity concentration of the disk-shaped lesion was 10 (arbitrary units), its radius was 1 cm and the width parameter, σ, of the Gaussian PSF was 0.3 cm (0.7 cm FWHM). The sinogram consisted of 128 projections, each containing 128 samples at 0.167-cm increments. For the 20-cm radius attenuator, the activity concentration of the lesion was 10, its radius was 1.67 cm and the width parameter, σ, of the Gaussian PSF was 0.5 cm (1.2 cm FWHM). The sinogram consisted of 256 projections, each containing 256 samples at 0.167-cm increments. Inversion of the (single-element) information matrix for the one-parameter model yielded the CRB for estimation of lesion activity when all other parameters are known. For the two-unknown-parameter model, the CRB was evaluated both for estimation of lesion activity when lesion size is unknown and for estimation of lesion size when activity is unknown.

Because in practice the size and shape of the attenuator will not match those assumed when defining the nonuniform sensitivity profiles, we tested the sensitivity of the results to variations in attenuator size and shape. We calculated the CRB for the SKE activity estimation task for an 8 × 5-cm (semiaxes) elliptical attenuator with the sensitivity functions derived assuming the 10-cm radius circular attenuator and for a 16 × 10-cm elliptical attenuator with the sensitivity functions derived assuming the 20-cm radius circular attenuator. The bound was evaluated for lesion locations along both the semimajor and the semiminor axes.

RESULTS

The values of the CRB for the three estimation tasks and the uniform collimator sensitivity profile, with and without attenuation, are shown in Figure 2. For a given task and lesion location, the ratio of the CRB with no photon attenuation to the CRB under more realistic conditions represents the increase in the lower bound on variance of the parameter estimate, or decrease in ideal performance, which can be attributed to attenuation. This degradation of performance was greatest when the lesion was located at the center of the phantom, and it was greater in the larger phantom than in the smaller phantom. Although the absolute levels of performance differed substantially among the three tasks, the ratios of variance with and without attenuation were nearly identical (Fig. 3). For the 10-cm-radius attenuator, the factor by which variance increased due to photon attenuation ranged from 4.5 at the phantom center to 2.0 at 1 cm from the edge; for the 20-cm-radius attenuator, the factor ranged from 20.0 at the center to 2.9 at 2 cm from the edge.

The nonuniform sensitivity profiles led to reductions in variance over most of the image area, up to radii of 8 cm in the 10-cm-radius attenuator and 16 cm in the 20-cm-radius attenu-

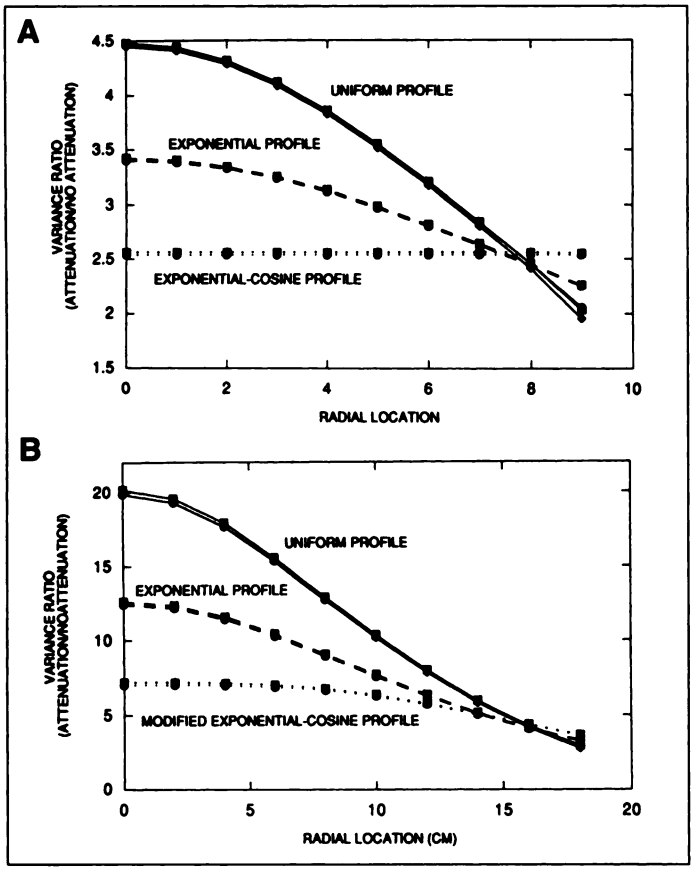

FIGURE 3. Increase in variance due to photon attenuation for three estimation tasks and three sensitivity profiles for a 10-cm (A) and 20-cm radius (B) attenuator. Estimation tasks and symbols are those used in Figure 2. Ratios of lower bounds on variance are almost identical for the three tasks; symbols are nearly superimposed.

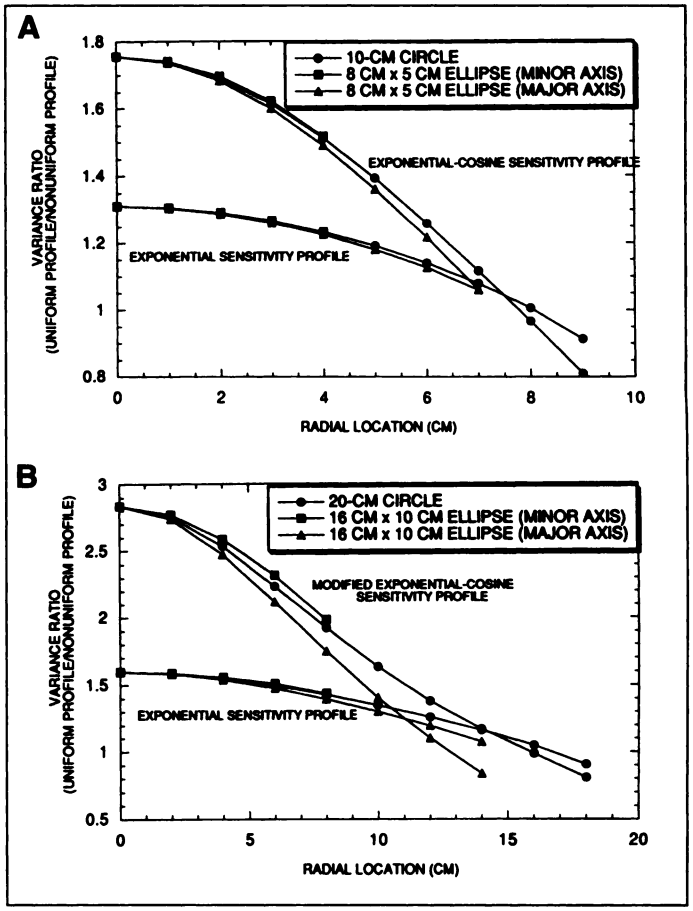

FIGURE 4. Sensitivity to assumed attenuator size and shape for the one-parameter activity estimation task for a 10-cm (A) radius attenuator and 8 x 5-cm elliptical attenuator with nonuniform sensitivity profiles derived assuming 10-cm and 20-cm (B) radius attenuators and 16 x 10-cm elliptical attenuator, with nonuniform sensitivity profiles derived assuming 20-cm radius attenuator. Performance was determined for lesion locations along both the major and minor axes of the ellipses.

ator; at larger radius, performance was degraded compared to that achieved using the uniform sensitivity profile (Fig. 3). As expected, the exponential-cosine sensitivity profile led to equal task performance throughout the 10-cm-radius attenuator. The modified exponential-cosine sensitivity profile, although not perfectly equalizing performance throughout the 20-cm-radius attenuator, led to more nearly equal performance compared to the uniform and exponential profiles. At the center of the smaller phantom, the exponential sensitivity profile reduced variance by a factor of 1.3, and the exponential-cosine sensitivity profile reduced variance by a factor of 1.8. At the center of the larger phantom, the exponential sensitivity profile reduced variance by a factor of 1.6, and the modified exponential-cosine sensitivity profile reduced variance by a factor of 2.8.

The effects of nonuniform collimator sensitivity on task performance were relatively insensitive to the assumptions about the size and shape of the attenuator. The centrally peaked sensitivity profiles led to improved estimation performance throughout most of the attenuator even when its shape deviated from that assumed when deriving the nonuniform sensitivity function (Fig. 4). Although task performance was better for the elliptical attenuators than for the larger circular attenuators, the ratios of performance with the nonuniform profiles to that with the uniform profile were similar.

DISCUSSION

We have quantified the effects on several estimation tasks of increased image noise due to loss by attenuation of emitted photons. For solid areas of the body, such as the brain and the abdomen, photon attenuation leads to a significant increase in image noise that is greatest in deep structures. This increase in noise can be mitigated by modifying the collimator to increase the detection fraction of photons emitted from central regions. A centrally peaked sensitivity function leads to reductions in image noise and, consequently, improvements in estimation task performance over most of the image at the expense of minor degradation in performance in peripheral regions. These improvements are gained with no increase in injected dose or imaging time. These findings imply that SPECT instruments with uniform collimator sensitivity are suboptimal in that they do not fully exploit the information available in the pattern of photons emitted from the patient. The improvements in quantitation tasks involving structures located deep within the brain or abdomen that can be achieved by modifying the collimator sensitivity profile are much greater than those to be gained by improved attenuation correction methods or image processing techniques.

We have determined values of the CRB from the attenuated sinogram (i.e., the fundamental measurements). These values represent the best possible performance (by an unbiased estimator that can be attained using these data). The precision that will actually be achieved for estimation from images will also depend on the attenuation correction method (if one is used), the reconstruction algorithm and the method used to estimate the quantities of interest.

Intrinsic attenuation correction algorithms require multiplication of each measured projection by a function that compen-

sates for photon attenuation between a line through the center of rotation, parallel to the detector and the (convex) external object contour nearest the detector. If a nonuniform sensitivity profile is used, then the measured projections must be multiplied by an appropriately modified function. Attenuation correction and image reconstruction can then proceed as usual. Premultiplication, or scaling, of the measured projections is often viewed as increasing the noise. A centrally peaked collimator sensitivity will greatly reduce the magnitude of the scaling. An alternate view is that the noise in a region of the image simply reflects the number of detected photons originating in that region. The nonuniform sensitivity profiles proposed here will increase that number throughout most of the image.

The effect of photon attenuation on performance in estimation tasks, and the gains from an improved data acquisition strategy, varied little among the tasks we considered. In previous studies using similar tasks, we have found that the effect of changes in collimator design depended strongly on the task being considered (*14–17*). These disparate results can be explained by the fact that previously we considered tradeoffs between aspects of image quality (e.g., resolution versus sensitivity), while in the current study a single aspect, sensitivity, is simply being reallocated within the projection.

Improvements in task performance over most of the image plane reflect increased detection of photons emitted from those regions; therefore, performance improvements would be expected in any quantitative task using SPECT data as well as in subjective tasks requiring human judgment (e.g., lesion detection). Performance in tasks involving extended distributions of radioactivity would be improved to a somewhat greater extent than were the tasks considered here, which involved small focal sources. For extended distributions of radioactivity, significantly more photons would be detected using the centrally peaked sensitivity profiles, reducing the overall level of noise in the projections.

For nonlinear tasks using very noisy images, the performance improvements to be gained by replacing the standard uniform sensitivity collimator with a nonuniform sensitivity collimator might be even greater than those reported here. It is well-known that for nonlinear tasks at low signal-to-noise ratio, the best possible performance represented by the CRB cannot be achieved by any estimator (*19*). We have previously reported that as noise levels increase, a threshold is reached where performance in estimation tasks deviates sharply from that predicted by the CRB (*18*). Therefore, reduction in noise levels that would bring the images into the regime where the CRB can be achieved could lead to even greater performance improvements, potentially converting marginal images to useful images.

While improvements in performance are realized over most of the scanning circle, variance is increased at the most peripheral locations. Performance in quantitative tasks that use only peripheral regions, such as those involving the brain cortex (*21*), would be degraded by the nonuniform sensitivity collimators described here. If only the peripheral regions are of interest, however, the uniform sensitivity profile, although better than the centrally peaked profiles, would not be optimal. Better performance would be attained using a nonuniform profile that is peaked at the edges. Conversely, if only the deep structures are of interest, then a profile more centrally peaked than those considered here, which concentrates sensitivity in those regions, would be preferred. However, for general-purpose imaging the best collimator would seem to be one that equalizes, as closely as possible, the variance thoughout the image.

Collimators with centrally peaked sensitivity functions are even more important for imaging isotopes, such as ^{201}Tl, whose attenuation coefficients are greater than that of ^{99m}Tc. Although a nonuniform sensitivity collimator designed for ^{99m}Tc would be better than a uniform sensitivity collimator for imaging other isotopes, ideally a collimator would be designed for each isotope being used.

Centrally peaked sensitivity profiles can be achieved using available technology. The CERASPECT system (Digital Scintigraphics, Inc., Waltham, MA) uses a cylindrical collimator assembly that rotates within a stationary cylindrical NaI(Tl) crystal. The standard collimator consists of three identical parallel-hole segments, each spanning the entire projection. The segmented collimator proposed by Genna and Smith (*6*) differs from the standard collimator in that it consists of six parallel-hole segments, only one of which covers the entire projection length. The other segments, which are shorter, collect data only from the central portion of the projection. This design accomplishes a discrete approximation to the exponential-cosine sensitivity profile. Although this design is unique to the cylindrical geometry of the CERASPECT dedicated brain scanner, collimators with centrally peaked sensitivity functions can also be achieved for planar cameras by variable-focus collimators such as the one designed by Hawman and Haines (*7*) for the purpose of avoiding truncation artifacts in cardiac imaging. If a change in sensitivity profile is associated with a change in spatial resolution, then this must be incorporated into the determination of task performance. In this case we would expect that evaluation of the merits of various collimator designs would be task dependent.

This report illustrates that the ideal-observer approach can be used to determine an optimal hardware configuration without the need for construction and testing of multiple alternative designs. We have previously determined the optimal balance between collimator resolution and sensitivity for nonlinear estimation tasks (*14,16,17*). Ideal-observer models of performance in linear detection tasks have been used by Barrett and Gifford (*22*) to optimize the data collection strategy for cone-beam tomography. Although they used the Cramer-Rao bound and the Fisher information matrix to quantify image information for particular tasks, their approach differs significantly from the one we have used here. In their implementation, the information matrix is based on estimation of the Fourier components of the image. The matrix is modified by a vector that weights these components by their importance for the task. In our approach this weighting is implicit in the information matrix, which pertains to the unknown parameters of the object and whose dimension changes with the task specification. For the linear SKE estimation task we considered, Barrett and Gifford's model would yield the same results as ours. Nonlinear tasks cannot be analyzed using their approach.

CONCLUSIONS

We have used ideal-observer models of estimation tasks to demonstrate that the standard collimator design, with uniform sensitivity along the projection, is suboptimal for most purposes and should be replaced by a collimator with a nonuniform sensitivity profile. Such collimators can be designed for most hardware configurations. The uniform-sensitivity collimator leads to suboptimal use of the information in the pattern of radioactivity emitted from the interior regions of the brain and abdomen.

APPENDIX

For a point source located at radial distance s (and angle 0) in a circularly attenuating phantom of radius r_o, the total sensitivity (i.e., integrated over the sinogram) is:

$$TS(s) = \int_0^{2\pi} \exp\left[-\mu\sqrt{r_0^2 - (s\cos\phi)^2} - \mu s\sin\phi\right] d\phi. \quad \text{Eq. A1}$$

One criterion for an optimized collimator sensitivity function is that it lead to equal total sensitivity at each point in the scanning circle, assuming a particular attenuator size, shape and attenuation coefficient. That is,

$$K = \int_0^{2\pi} CS(s\cos\phi)\exp\left[-\mu\sqrt{r_0^2 - (s\cos\phi)^2} - \mu s\sin\phi\right] d\phi, \quad \text{Eq. A2}$$

where CS(x) is the collimator sensitivity function and K is a constant. It is clear that Equation A2 can be satisfied by

$$CS(s) = f(x)\exp\left[\mu\sqrt{r_0^2 - x^2}\right] \quad \text{Eq. A3}$$

if a function f(x) can be found such that

$$K = \int_0^{2\pi} f(s\cos\phi)\exp\left[\mu s\sin\phi\right] d\phi. \quad \text{Eq. A4}$$

This condition can be satisfied by (*23*):

$$f(x) = \cos(\mu x). \quad \text{Eq. A5}$$

The collimator sensitivity function that yields equal sensitivity at all points in a circularly-shaped attenuator of radius r_o and attenuation coefficient μ is:

$$CS(x) = K_{ec}\exp\left[\mu\sqrt{r_0^2 - x^2}\right]\cos(\mu x), \quad \text{Eq. A6}$$

where K_{ec} is a normalization constant that leads to sensitivity, integrated along the projection, equal to that of the uniform sensitivity profile.

ACKNOWLEDGMENTS

We are grateful to Dr. Sebastian Genna for recommending this problem to us, Dr. B. Leonard Holman for valuable suggestions and Sally Ann Edwards for editorial assistance. Part of this work was presented at the 1992 annual meeting of the Society of Nuclear Medicine. This research was supported by the United States Public Health Service grants R01 NS 31902 and R01 CA 55174.

REFERENCES

1. Bellini S, Piacentini M, Cafforio C, Rocca F. Compensation of tissue absorption in emission tomography. *IEEE Trans Acoustics Speech Signal Proc* 1979;ASSP-27:213–218.
2. Tretiak O, Metz C. The exponential radon transform. *SIAM J Appl Math* 39:341–354.
3. Gullberg GT, Budinger TF. The use of filtering methods to compensate for constant attenuation in SPECT. *IEEE Trans Biomed Eng* 1981;BME-28:142–157.
4. Hawkins WG, Leichner PK, Yang N-C. The circular harmonic transform for SPECT reconstruction and boundary conditions on the Fourier transform of the sinogram. *IEEE Trans Med Imag* 1988;7:135–148.
5. Metz CE, Pan X. A unified analysis of exact methods of inverting the 2-D radon transform with implications for noise control in SPECT. *IEEE Trans Med Imag* 1995;14:643–658.
6. Genna S, Smith AP. The development of ASPECT, an annular single crystal brain camera for high efficiency SPECT. *IEEE Trans Nucl Sci* 1988;NS-35:654–658.
7. Hawman PC, Haines EJ. The cardiofocal collimator: a variable-focus collimator for cardiac SPECT. *Phys Med Biol* 1994;39:439–450.
8. Wagner RF, Brown DG. Unified SNR analysis of medical imaging systems. *Phys Med Biol* 1985;30:498–518.
9. Burgess AE, Wagner RF, Jennings RJ, Barlow HB. Efficiency of human visual signal discrimination. *Science* 1981;214:93–94.
10. Judy PF, Swensson RG, Szulc M. Lesion detection and signal-to-noise ratio in CT images. *Med Phys* 1981;8:13–23.
11. Barrett HH. Objective assessment of image quality: effects of quantum noise and object variability. *J Opt Soc Am A* 1990;7:1266–1278.
12. Hanson KM. Method of evaluating image-recovery algorithms based on task performance. *J Opt Soc Am A* 1990;7:1294–1304.
13. Myers KJ, Rolland JP, Barrett HH, Wagner RF. Aperture optimization for emission imaging: effect of a spatially varying background. *J Opt Soc Am A* 1990;7:1279–1293.
14. Mueller SP, Kijewski MF, Moore SC, Holman BL. Maximum-likelihood estimation–a mathematical model for quantitation in nuclear medicine. *J Nucl Med* 1990;31:1693–1701.
15. Kijewski M, Mueller S, Moore S, Rybicki F. Generalized ideal-observer models for design and evaluation of medical imaging systems. *Radiology* 1990;177:208.
16. Kijewski MF, Mueller SP, Rybicki FJ, Carvalho PA. Very high precision inversion of ill-conditioned matrices: a medical imaging application. *Mathematica J* 1990;1:21–26.
17. Moore SC, deVries DJ, Nandram B, Kijewski MF, Mueller SP. Collimator optimization for lesion detection incorporating prior information about lesion size. *Med Phys* 1995;22:703–713.
18. Mueller SP, Kijewski MF, Kappeler C, Moore SC. Estimation performance at low SNR; predictions of the Barankin bound. *Proc SPIE* 1995;2432:152–166.
19. Van Trees H. *Detection, estimation and modulation theory*, vol. I. New York: Wiley: 1968.
20. Bracewell RN. *The Fourier transform and its applications*. New York: McGraw Hill: 1978.
21. Johnson KA, Kijewski MF, Becker JA, Garada B, Satlin A, Holman BL. Quantitative brain SPECT imaging in Alzheimer's disease and normal aging. *J Nucl Med* 1993;34:2044–2048.
22. Barrett HH, Gifford H. Cone-beam tomography with discrete datasets. *Phys Med Biol* 1994;39:451–476.
23. Gradshteyn IS, Ryzhik IM. *Table of integrals, series and products*. New York, NY; Academic Press: 1980.